Model infrared spectra for accreting stars

Bedijn, P.J.; Jong, T. de; Habing, H.J.

Astron. Astrophys. 69, 73—84 (1978)

ASTRONOMY AND ASTROPHYSICS

Model Infrared Spectra for Accreting Stars

P. J. Bedijn[1]*, H. J. Habing[1]** and T. de Jong[2]

[1] Sterrewacht, Huygens Laboratorium, Wassenaarseweg 78, Leiden, The Netherlands
[2] Sterrenkundig Instituut, Universiteit van Amsterdam, Roetersstraat 15, Amsterdam, The Netherlands

Received October 18, 1977

Summary. We have calculated infrared spectra for dusty circumstellar shells that accrete onto stars in free fall. The dust consists of silicate and graphite particles. We solve simultaneously the equation of radiative transfer and the two equations of thermal equilibrium, one for each of the dust species. In four cases (BN object; OMC 2/IRS 3; RCW 57/IRS 1; Mon R 2/IRS 2) model spectra are compared with spectra of observed infrared point sources. In each case good agreement between observation and prediction is obtained for a wide range of models. By using additional criteria (1. radiation pressure does not stop the inflow; 2. A_v/τ_{10} should be larger than 10) we are able to narrow the range of permissible models and to obtain an estimate of the accretion rate $\dot{M}$. Given the accretion time $M/\dot{M} \gtrsim 10^6$ yr and the number of similar objects known we conclude tentatively, that the four objects are very young early type stars at the end of their accretion phase.

Key words: star formation — circumstellar shells — accretion

1. Introduction

During the past ten years an increasing number of infrared point sources have been discovered, whose emission peaks are at wavelengths $\lambda < 20$ μm. Most of such infrared sources have been identified with warm dust shells surrounding (super) giant stars of late spectral type. However, a fair number do not fit into this category. They are generally found in regions of the sky where star formation takes place, such as in extended dark dust clouds, in regions of molecular line radiation, near compact H II regions and in OB and *T* associations. We assume therefore that the IR point sources also are rather young objects.

Some of the young IR sources have turned out to be very reddened O stars (W 3 – IRS 1A is an example), but others have spectra that indicate that emitting dust surrounds the source(s) of energy. Among those, a distinct group appears, which may be named after its prototype, the BN object, discovered by Becklin and Neugebauer (1967). The group properties of BN type objects appear to be the following:

1. The sources are less than a few arc s in size.
2. The continuum spectrum resembles that of the BN object—sharply rising at $\lambda < 8$ μm, turning over at around 9 μm and roughly constant between $\lambda = 10$ μm and $\lambda = 20$ μm.
3. The sources have considerable optical depth in the 9.7 μm feature.
4. Compact or ultra-compact H II regions may appear in the surroundings but they are never directly associated with the IR source.
5. OH, H_2O and (possibly) SiO masers may occur very close to the sources. If an OH maser occurs it is of type I.
6. The sources are found in regions of molecular activity. A tentative list of objects that fulfil these criteria has been given by Matthews et al. (1977).

In this paper we discuss a simple model that can explain the infrared spectra of the BN type sources. We assume, as did Becklin and Neugebauer (1967), that the objects involved are very young. We therefore reject the hypothesis of Penston et al. (1971) that the BN object is a very luminous star of intermediate spectral type, accidentally seen through a large dust cloud. The known existence of a sizeable number of similar sources within a few kpc from the Sun argues strongly against a chance coincidence.

The foundation of our model comes from theoretical studies of the formation of stars through the gravitational collapse of a cloud of dust and gas (Larson, 1969a, 1972; Westbrook and Tarter, 1975). These

Send offprint requests to: P. J. Bedijn
* Now at Max-Planck-Institut für Physik und Astrophysik, München, Germany.
** Visiting Fellow, 1976–1977, Joint Institute for Laboratory Astrophysics, University of Colorado and National Bureau of Standards, Boulder, Colorado

studies have shown that very soon after the onset of collapse a central stellar core is formed. For large initial cloud masses the central object may evolve into a massive main-sequence star while still surrounded by a large amount of infalling dust and gas (Appenzeller and Tscharnuter, 1974; Kahn, 1974). The visual and ultraviolet radiation of the central star is completely absorbed by this opaque dust shell and is reemitted at infrared wavelengths. It seems quite probable that even though the star has reached its main-sequence position the formation of an H II region around the star is prevented by the inflow of gas and dust (Larson and Starrfield, 1971; Kahn, 1974). We will refer to these objects as "accreting young stars". The term "cocoon star" has been used (Kahn, 1974) for such an accreting star; however, we think that this usage is confusing since originally the term "cocoon star" has been used for dense dust shells surrounding very small H II regions (Davidson and Harwit, 1967; Cochran and Ostriker, 1977). The "cocoon star" therefore appears to represent a slightly later phase in the stellar evolution than the accretion phase.

The first calculations of the infrared spectra of accreting young stars have been made by Larson (1969b). Larson compared his predictions with the then known observations of the BN object. More recent observations, especially around the 9.7 μm feature and at 20 μm, show considerable differences with Larson's predictions.

Basically our model is the same as that of Larson. We calculate the infrared spectrum emerging from a large dust sphere that surrounds a point-like energy source. The density in the dust sphere varies as $r^{-3/2}$, corresponding to a cloud collapsing with free fall speed. As compared to Larson we make the following changes and additions.

(i) We assume that more than one kind of dust is present in the cocoon (in our present calculations graphite and silicate dust). Throughout the envelope each kind of dust has its own temperature distribution that is determined by the balance between absorption and emission of radiation.

(ii) We solve simultaneously the equation of radiative transfer and the two equations of thermal equilibrium, one for each kind of dust.

(iii) The immediate surroundings of the central star will be free of dust. When dust grains come too close to the central star, their temperatures rise above the dust melting temperature and they will therefore evaporate. The opacity of the gas is much lower and it is therefore assumed that stellar radiation can flow freely through the dustless cavity.

(iv) The radiation emerging from the shell is attenuated by the dust in its surrounding parent cloud. This "exterior extinction" will be taken into account in our model.

A preliminary account of our results has been given by Bedijn et al. (1977) and in Bedijn (1977a). A related, recent paper is by Finn and Simon (1977). They also calculate infrared spectra of point-like sources seen through very dense circumstellar shells. However, Finn and Simon make quite a few assumptions different from those in our paper: their source of energy (the central star) is a cool blackbody; they assume only one type of grain (silicates) and do not include exterior extinction explicitly.

Our paper is organized as follows. In Section 2 the radiative transfer in a spherical dust shell is discussed. In Section 3 we specify the opacity properties of the dust in the shell and of the dust responsible for the foreground extinction. In Section 4 we describe our model fitting procedure. In Section 5 we present fits to a number of observed sources and in Section 6 the results are discussed.

2. Radiative Transfer in a Spherical Dust Shell

As has been outlined in Section 1, we consider a spherical dust shell that contains two kinds of dust, graphite and silicate particles. In the shell the density of gas and dust is given by $\rho=\rho_0 r^{-3/2}$. The radiation of a central star of total luminosity L impinges on the inner boundary of the dust shell and is subsequently converted to infrared wavelengths by absorption and reemission by the dust inside the shell. The central star is assumed to be a point source. We want to calculate the spectral distribution of the flux leaving the outer radius of the shell, assuming that inside the shell radiative energy is being conserved. It has been shown by one of us (Bedijn, 1977a, b) that inside the shell one can write for the monochromatic mean intensity of the infrared radiation field

$$J_\lambda(r)=\tfrac{1}{2}\int_{r_{\rm in}}^{r_{\rm out}}\rho(r')r'^2\cdot\sum_i \varkappa_a^i(\lambda)\cdot B_\lambda[T_i(r')]\cdot E_1^{sp}(r',r,\lambda)dr'. \quad (1)$$

Here $\rho(r')$ is the mass density of gas and dust, $\varkappa_a^i(\lambda)$ is the mass absorption coefficient of the i^{th} kind of dust per unit mass of the gas-dust mixture, $T_i(r')$ is the temperature of the i^{th} kind of dust, B_λ is the Planck function, and $r_{\rm in}$ and $r_{\rm out}$ are the inner and outer boundaries of the dust shell. The function E_1^{sp}, the spherical analogue of the first exponential integral E_1, weights the contribution of a thin spherical shell at r' to the mean intensity at r. E_1^{sp} depends only on the optical properties and the geometrical distribution of the dust and has been given in explicit form in Bedijn (1977a). We neglect scattering by dust grains.

Equation (1) has to be solved under the condition that the two temperature distributions $T_i(r)$ each satisfy the relation of conservation of radiative energy:

$$\varkappa_a^i(\mathrm{UV})\,\frac{L}{(4\pi r)^2}\exp\left[-\tau_{\rm UV}(r)\right]+\int_{\rm IR}\varkappa_a^i(\lambda)\cdot[J_\lambda(r)-B_\lambda(T_i,r)]d\lambda=0. \quad (2)$$

The first term represents heating of the dust grains directly by stellar light. τ_{UV} is the ultraviolet optical depth of the dust and is measured from the inner radius r_{in} in the outward direction. Since we assume grey absorption in the ultraviolet, the shape of the stellar spectrum is immaterial in our calculations, as long as the star is sufficiently hot. Once we have obtained temperature distributions $T_i(r)$ consistent with Equations (1) and (2) we then calculate the monochromatic Eddington flux of the infrared radiation field (cf. Mihalas, 1970; pp. 4 and 5)

$$H_\lambda(r)=\tfrac{1}{2}\int_{r_{in}}^{r_{out}}\rho(r')r'^2\sum_i \kappa_a^i(\lambda)B_\lambda[T_i(r')]E_2^{sp}(r', r, \lambda)dr'\lambda, \tag{3}$$

where $E_2^{sp}(r', r, \lambda)$ is the spherical analogue of the second exponential integral E_2. An explicit expression for E_2 may be found in Bedijn (1977a, b).

Radiative equilibrium, Condition (2), also implies conservation of radiative flux which we can write as

$$\frac{L}{(4\pi r)^2}\{\exp[-\tau_{UV}(r)]-1\}+\int_{IR} H_\lambda d\lambda=0 \tag{4}$$

for all r. Equation (4) can be used as a check on the accuracy with which the radiative transfer is solved numerically. We are especially interested in the infrared flux density leaving the system at r_{out}, integrated over the whole sphere. Therefore we define $L_\lambda(\text{out})\equiv(4\pi r_{out})^2 H_\lambda(r_{out})$, and we will call this the "intrinsic" spectrum of the object, since it is not yet modified by extinction outsider r_{out}.

A fundamental step preceding the calculations is the determination of the dust opacities $\kappa_a^i(\lambda)$. This problem will be discussed at some length in the next section. As a first step in the numerical solution of the radiative transfer we fix the inner and outer boundaries of the shell. There are two inner boundaries to consider: the distance $r_{m,g}$ at which the graphite particles melt, and the distance $r_{m,s}$ where the silicate particles melt. Since the graphite grains melt at a higher temperature than the silicate grains (cf. Section 3) they can come closer to the central star. Thus we determined the innermost boundary $r_{in}=r_{m,gr}$, the radius of the melting surface of graphite, by the relation

$$\kappa_a^g(\text{UV})\frac{L}{(4\pi r_{m,g})^2}-\int_{IR}\kappa_a^g(\lambda)B_\lambda(T_{m,g})d\lambda=0, \tag{5}$$

where $T_{m,g}$ is the melting temperature of graphite. The use of Equation (5) neglects heating of graphite grains at $r_{m,g}$ by absorption of infrared radiation generated in the shell. *A posteriori* we found this to be a good approximation. The radius of the melting surface of silicate grains, $r_{m,s}$, has to be determined in an iterative manner because (i) the stellar radiation at $r_{m,s}$ is attenuated due to absorption by graphite grains between $r_{m,g}$ and $r_{m,s}$ and (ii) the heating of the silicate grains at $r_{m,s}$ by the infrared radiation of the shell cannot be neglected (back heating). We determine $r_{m,s}$ from

$$\kappa_a^s(\text{UV})\frac{L\exp[-\tau'_{UV}]}{(4\pi r_{m,s}^2)}-\int_{IR}\kappa_a^s(\lambda)B_\lambda(T_{m,s})d\lambda=0 \tag{6}$$

and

$$\tau'_{UV}=2\kappa_a^g(\text{UV})\rho_0(r_{m,g}^{-1/2}-r_{m,s}^{-1/2}). \tag{7}$$

The back heating can be taken into account by choosing for $T_{m,s}$ a value lower than the actual melting temperature (up to a factor of 3 smaller in some cases) such that the actual temperature of the silicate particles at $r_{m,s}$ equals the melting temperature. Finally the outer boundary is arbitrarily set at $r_{out}=1000\,r_{in}$.

After this first step several others have to be taken. We choose a grid of 21 radial points between r_{in} and r_{out}. Five points are equidistantly placed between the graphite and silicate melting radii. For the remaining 16 points the distance between adjacent gridpoints, $r_{j+1}-r_j$, increases smoothly upon approaching r_{out}. We specify a grid of 80 wavelength points, logarithmically spaced between 0.5 μm and 40 μm. The wavelength boundaries have been chosen such that throughout the dust shell an insignificant fraction of the infrared radiation falls outside this wavelength range. Once the dust density distributions and absorption properties have been specified we can evaluate the weight functions E_1^{sp} and E_2^{sp} at all radial and wavelength grid points. Choosing dust temperature distributions $T_i(r_j)$ we then calculate the monochromatic mean intensity $J_\lambda(r)$ and the Eddington flux $H_\lambda(r)$ at all radial and wavelength grid points by numerical calculation of Equations (1) and (3). Performing the wavelength integration it is then verified whether the choice $T_i(r_j)$ satisfies radiative equilibrium, Condition (2), at all radial grid points. Usually this is not the case and a Λ-iteration on both temperature distributions is carried out until Condition (2) is satisfied within 2%. For a reasonable initial choice of $T_i(r_j)$ this is usually achieved with 6 iterations, that take about 7 min CPU time on the IBM 370/158 of Leiden University. Flux conservation, Condition (4), is satisfied within 3% in all cases calculated.

3. Dust Properties

A lot of information on the optical properties of solid grains in the interstellar medium can be extracted from the observed extinction curve between 0.3 μm^{-1} and 9 μm^{-1}. First, it seems that more than one kind of dust is responsible for the interstellar extinction (see e.g. the review by Aannestad and Purcell, 1973). The presence of solid particles of graphite and silicate seems well established. Gilra (1971) and Savage (1976) have shown that spherical particles of graphite with an average radius of 0.025 μm can explain the 2200 Å bump in the interstellar extinction curve. The severe limitations on

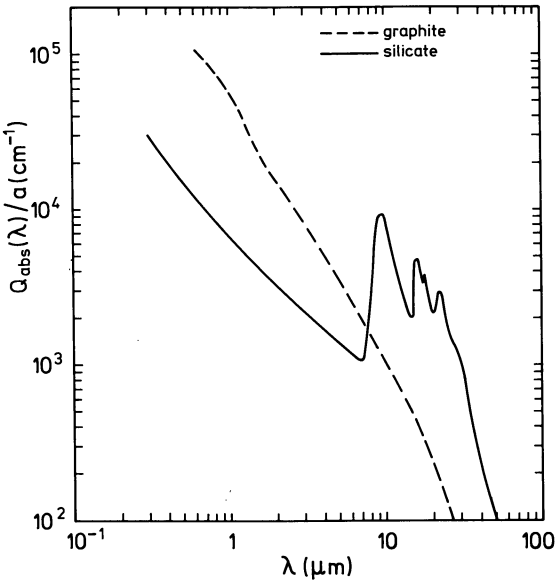

Fig. 1. Adopted absorption efficiencies of graphite and silicate grains

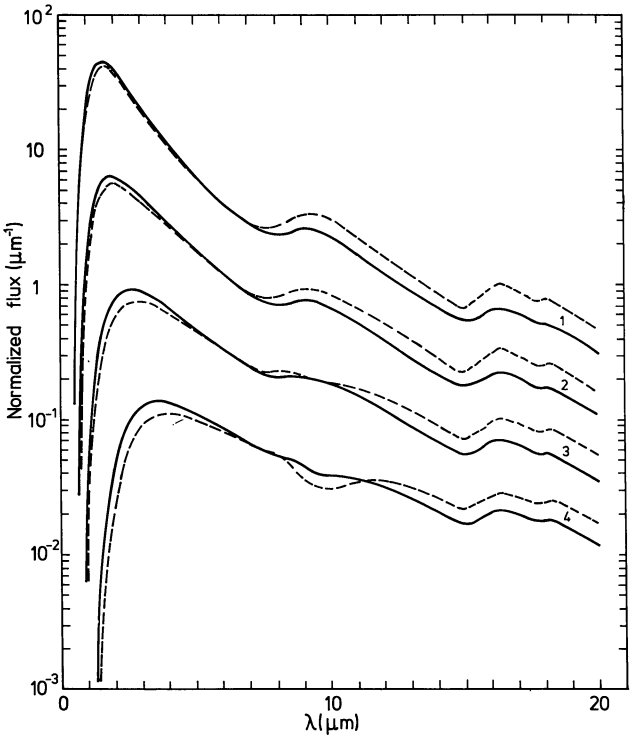

Fig. 2. Normalized intrinsic infrared spectra for the parameters in Table 1. Solid curves are for $\delta_s/\delta_g=1.5$, dashed curves for $\delta_s/\delta_g=3$. For convenient display, Spectra 1 to 3 are shifted up by a factor of 5 with respect to each other

the size distribution required by Savage are no longer necessary (Mathis, private communication). Interstellar silicate has been identified through its 10 μm absorption band as observed towards compact H II regions, towards the galactic center, and towards the sources discussed in this paper. These observations demonstrate the existence of silicates in rather special regions. The only evidence for the existence of silicate dust in the general interstellar medium is the observation of the 10 μm absorption feature towards the star VI Cygni 12 (Rieke, 1974; Gillett et al., 1975a).

In general it appears that not enough graphite and silicate dust particles exist to explain the observed visual extinction. About 30 yr ago van de Hulst (1949) suggested that so-called "dirty ice" particles are responsible for the extinction at visual wavelengths. The chemical composition of this material is uncertain but in order to explain the observed extinction it has to be dielectric. One imagines that this material is quite volatile and condenses out on pre-existing graphite and/or silicate particles as "dirty ice" mantles (Greenberg and Hong, 1974). In this paper we assume that the extinction in the dark dust cloud surrounding the accreting star is caused by a mixture of three kinds of dust particles: graphite, silicate and "dirty ice" (to be referred to as foreground extinction). In the warm dust shell "dirty ice" will be evaporated so that only graphite and silicate remain. The existence of ice particles or ice mantles on other particles is strongly supported by the observation (Soifer et al., 1976) that objects hidden in dense clouds show an absorption band probably due to H_2O ice. However, the absence of this band outside dense clouds remains a puzzle in view of what has been said before.

i) Graphite

We take spherical graphite particles of radius $a_g=0.02$ μm. Infrared absorption efficiencies $Q^g_{abs}(\lambda)$ of these particles were calculated with Mie theory using the optical constants of graphite determined by Taft and Phillipp (1965). The mass absorption coefficient per unit mass of the dust-gas mixture is $\varkappa^g_a(\lambda)=3\delta_g Q^g_{abs}(\lambda)/4s_g a_g$; δ_g is the dust to gas mass abundance ratio for graphite, $s_g=2.5$ g cm^{-3} is the graphite specific weight. Because in the infrared $2\pi a/\lambda \ll 1$, $Q^g_{abs}(\lambda)/a_g$ and thus $\varkappa$ are independent of the particle radius (Rayleigh approximation). Figure 1 shows $Q^g_{abs}(\lambda)/a_g$ as a function of λ (dashed curve).

We assume that the UV absorption efficiency is unity. This is a reasonable average value for a blackbody spectral energy distribution at a temperature of about 30000 K. In any case, the actual spectral distribution of radiation from the central star is unknown. The ultraviolet mass absorption coefficient equals $\varkappa^g_a(\mathrm{UV})=3\delta_g/4s_g a_g=1.5\,10^5\,\delta_g$ cm^2 g^{-1}.

Scattering by dust grains is neglected altogether. For the adopted particle size this is a good approximation at infrared wavelengths. However, at ultraviolet wavelengths scattering and absorption can be of the same order of magnitude. Luckily, scattering will not have a large effect on the distribution of UV stellar photons in

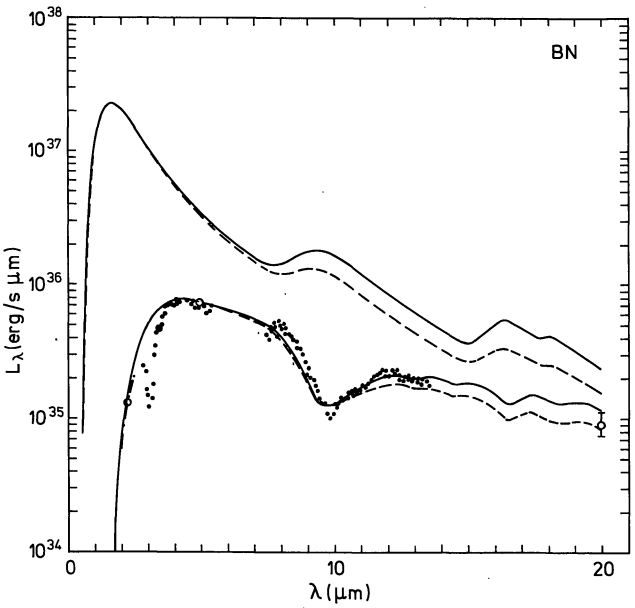

Fig. 3. Theoretical infrared spectra for the BN object based on Spectra 1 of Figure 2 without (upper curves) and with (lower curves) exterior extinction. Dashed curves are for $\delta_s/\delta_g = 1.5$ and solid curves for $\delta_s/\delta_g = 3$. Observations shown are: 2.2 μm, 3.5 μm, 4.8 μm and 20 μm broad band photometric luminosities (open circles), 2 μm to 2.4 μm spectrophotometric luminosities (dash-dotted curve), and 3 μm to 5 μm and 8 μm to 14 μm spectrophotometric luminosities (black dots)

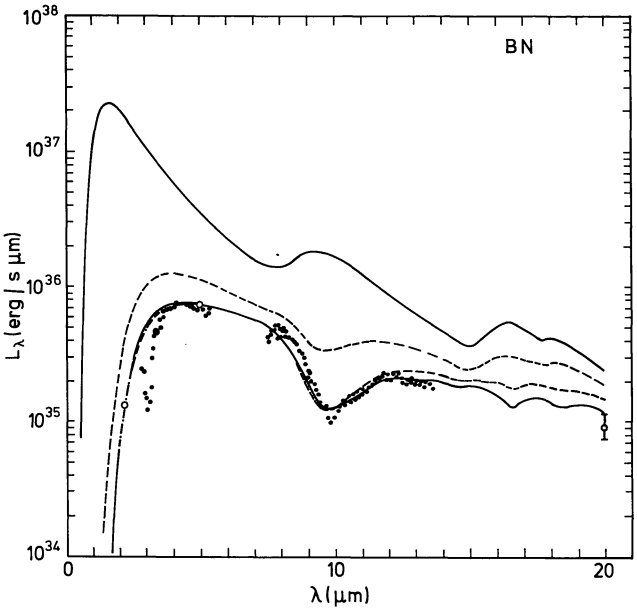

Fig. 4. The same as Figure 3, but now predicted spectra are based on Spectrum 1 of Figure 2 with $\delta_s/\delta_g = 3$ (solid curves) and Spectrum 4 of Figure 2 with $\delta_s/\delta_g = 3$ (dashed curves)

Table 1. Parameters of the theoretical spectra of Figure 2

	Spectrum no.	$\rho_0\delta_g L^{-1/4}$ (g cm$^{-3/2}$ erg$^{-1/4}$ s$^{1/4}$)	τ_{UV}	$\tau_{1\,\mu m}$	$\tau_{10\,\mu m}$	$r_{0.9}/r_{in}$		
						5 μm	10 μm	20 μm
$\frac{\delta_s}{\delta_g}=1.5$	1	$1.42\,10^{-7}$	12.3	1.1	0.18	9.3	43	210
	2	$2.8\,10^{-7}$	26	2.3	0.42	8	35	180
	3	$5.7\,10^{-7}$	53	4.6	0.90	7	30	145
	4	$1.14\,10^{-6}$	108	9.2	1.86	6.2	27	130
$\frac{\delta_s}{\delta_g}=3.0$	1	$1.42\,10^{-7}$	15.9	1.24	0.34	8.5	33	180
	2	$2.8\,10^{-7}$	34	2.6	0.80	7.8	27	150
	3	$5.7\,10^{-7}$	72	5.3	1.72	6.3	26	120
	4	$1.14\,10^{-6}$	146	10.6	3.6	5.9	30	110

the dust shell since scattering is highly forward peaked if $2\pi a \simeq \lambda$ (van de Hulst, 1957).

Finally we assume that the graphite grains melt suddenly at a temperature of 2000 K. This temperature follows from considering a graphite solid-vapor system in thermal equilibrium at vapor pressures to be expected in the inner regions of the dust shell.

ii) Silicate

We take spherical silicate particles of radius $a_s = 0.05$ μm. This value of a_s is about the upper limit to the size of silicate grains in the general interstellar medium (Hong, 1975). Infrared absorption efficiencies $Q^s_{abs}(\lambda)$ are calculated with Mie theory using the optical constants for andesite (Pollack et al., 1973) with the following modifications: (i) for $\lambda < 7.5$ μm we assume that the imaginary part of the index of refraction equals $k = 0.05$ and (ii) the 8 μm to 13 μm profile of andesite has been replaced by a profile as derived by Gillett et al. (1975b) with conservation of the integrated band strength. Modification (i) derives from the work of Jones and Merrill (1976) and Bedijn (1977a, b) who have demonstrated that the absorptivity at $\lambda < 7.5$ μm of silicates in the envelopes of cool M-type (super)giants must be enhanced with respect to terrestrial silicates in order to reproduce the observed infrared excesses.

Figure 1 shows $Q^s_{abs}(\lambda)/a_s$ as a function of λ (solid curve). From $Q^s_{abs}(\lambda)/a_s$ we can again derive the mass absorption coefficient per unit mass of the dust-gas

mixture $\varkappa_a^s(\lambda)=3\delta_s Q_{\rm abs}^s(\lambda)/4s_s a_s$; δ_s is the mass abundance ratio of silicate to gas and $s_s=2.47$ g/cm^3 is the adopted specific weight of silicate. Again the infrared mass absorption coefficient is independent of the precise particle size since $2\pi a/\lambda \ll 1$. Scattering by silicate grains has been neglected. Just like for graphite we assume a grey ultraviolet absorption efficiency of unity, so that the UV mass absorption coefficient becomes $\varkappa_a^s(\mathrm{UV})=3\delta_s/4s_s a_s=6.07\ 10^4\ \delta_s$ cm^2/g for $a_s=0.05$ μm. Silicates melt at 1000 K.

iii) Foreground Dust

The extinction properties of dust in the cool outer parts of the cocoon and in the surrounding dense cloud remain to be determined. We assume that three kinds of dust are together causing the foreground extinction: graphite, silicate and the more volatile "dirty ice".

The normalized extinction due to graphite and silicate dust, $A_1(\lambda)$, can be straightforwardly calculated from the absorption efficiencies shown in Figure 1

$$A_1(\lambda)=\left[\frac{s_g\delta_s}{s_s\delta_g}\,\frac{Q_{\rm abs}^s(\lambda)}{a_s}+\frac{Q_{\rm abs}^g(\lambda)}{a_g}\right]\Bigg/\left[\frac{s_g\delta_s}{s_s\delta_g}\,\frac{Q_{\rm abs}^s(V)}{a_s}+\frac{Q_{\rm abs}^g(V)}{a_g}\right]. \tag{8}$$

where δ_s/δ_g is restricted to have the same value as in the dust cocoon and where V stands for $\lambda=0.55$ μm. Note that the normalized extinction $A_1(\lambda)$ is not defined in the usual way; it is the extinction in magnitudes at wavelength λ when the extinction at V is unity.

From measurements of Brackett lines of hydrogen and comparison with radio continuum data several observers have been able to derive absolute values of the extinction up to $\lambda=4$ μm. The results show (Neugebauer, private communication) that the extinction follows rather closely van de Hulst's curve #15 (van de Hulst, 1949). We adopt this same theoretical extinction curve for the "dirty ice" particles and have recalculated values for Q at many more wavelength points in the IR. It turns out that in the wavelength region, where extinction according to the v.d. Hulst curve #15 contributes significantly to the total extinction, its wavelength dependence is quite similar to that of the combined graphite and silicate extinction. Therefore it is probably immaterial whether the "dirty ice" is deposited as mantles on some small fraction of the silicate and graphite particles or whether it occurs in pure "dirty ice" particles (Greenberg and Hong, 1974).

The total extinction $A(\lambda)$ is a linear combination of silicate and graphite extinction $A_1(\lambda)$ and v.d. Hulst #15 extinction $A_2(\lambda)$

$$A(\lambda)=\alpha A_1(\lambda)+\beta A_2(\lambda), \tag{9}$$

where α and β are free parameters to be determined when we fit model infrared spectra to actual observed spectra. $A(\lambda)$ is the total amount of extinction in magnitudes at a wavelength λ, when the total visual extinction amounts to $(\alpha+\beta)$ magnitudes.

4. Model Fitting Procedure

In Section 2 we described our dust shell model and the method of solution of the radiative transfer. The infrared spectrum emerging from such a dust shell depends on the following free parameters: the total luminosity of the central star L, the scale factor ρ_0 of the radial density distribution of dust and gas and the dust to gas mass abundance ratios of graphite and silicate, δ_g and δ_s.

Luckily, not every combination of L, ρ_0, δ_g and δ_s gives an independent spectrum. It has been shown by Bedijn (1977a, b) that under certain conditions the shape of the outgoing spectrum $L_\lambda(\mathrm{out})/L$ is independent of variations in the free parameters. Actually $L_\lambda(\mathrm{out})/L$ remains constant under variations of L, ρ_0, δ_g, δ_s if the following conditions are met:

(i) dust and gas have a r^n power law density distribution

(ii) $\rho_0\delta_g L^{(n+1)/2}$ is kept constant ($=\rho_0\delta_g L^{-1/4}$ if $n=-3/2$)

(iii) δ_s/δ_g is kept constant

(iv) $r_{\rm in}/r_{\rm out}$ is kept constant

(v) the input stellar spectrum retains the same shape.

Condition (v) is rather unimportant in our case, since we assume that the opacity for direct stellar radiation is grey. Also Condition (iv) is only moderately important since $L_\lambda(\mathrm{out})$ is only slightly dependent on the exact value of $r_{\rm out}$, as long as $r_{\rm out}$ is sufficiently large. It therefore appears that the actual free parameters of our model dust shell are the two combinations $\rho_0\delta_g L^{-1/4}$ and δ_s/δ_g.

Some examples of normalized theoretical infrared spectra are shown in Figure 2. They were calculated for the values of $\rho_0\delta_g L^{-1/4}$ given in Table 1, for $\delta_s/\delta_g=1.5$ (solid curves), and for $\delta_s/\delta_g=3$ (dashed curves). In Table 1 we also give the total optical depths of the dust shell for stellar radiation $\tau_{1\mu\mathrm{V}}$, and the optical depths at a few infrared wavelengths. In the last three columns we give the radii of the circular disks that contain 90% of the infrared flux at the three wavelengths indicated, $r_{0.9}$, in units of the inner radius of the dust shell, $r_{\rm in}=1.38\ 10^{12}\ (L/L_\odot)^{1/2}$ cm (see Eq. A9). These radii are used to calculate predicted angular sizes of some sources. The spectra calculated with $\delta_s/\delta_g=1.5$ (solid curves in Fig. 2) and the spectra calculated with $\delta_s/\delta_g=3$ (dashed curves) differ in shape. There is less emission at $\lambda<6$ μm and more emission at $\lambda\gtrsim 7$ μm in the spectra with relatively more silicate (larger δ_s/δ_g). Due to the increase of the amount of silicate dust relative to the amount of graphite dust the optical depth of the dust shell becomes

larger at all wavelengths. Radiation at shorter wavelengths is mainly due to graphite deep inside the atmosphere and therefore it is more attenuated in case of higher silicate abundances. The decrease of emerging radiation at the shorter wavelengths has to be counterbalanced by an increase of emerging radiation at the longer wavelengths. In spectrum 4 of Figure 2 a larger amount of silicates leads to a decrease in flux between 8 μm and 11 μm. In that case the optical depth between 8 μm and 11 μm is so large that self-absorption becomes important. It will be shown in Section 5 that the influence of δ_s/δ_g on the spectral shape of the emerging radiation can be successfully used to determine its value, when the theoretical spectra are compared with observations.

If the flux density from the source at Earth is $S(\lambda)$, and the distance of the source is d we can write

$$S(\lambda)=\left(\frac{L_\lambda(\text{out})}{L}\right)\frac{L}{4\pi d^2}\exp\left[-0.921\,A(\lambda)\right]. \quad (10)$$

The factor 0.921 arises from the transformation of magnitude to optical depth. $S(\lambda)$ can be compared directly to observed values. If we select one of the normalized spectra, $L_\lambda(\text{out})/L$, shown in Figure 2, the righthand side of (10) still contains three unknowns: $L/4\pi d^2$, α and β [cf. Equation (9)]. To determine these three unknowns we demand that at three different wavelengths the predicted value of $S(\lambda)$ agrees with the observed value. An eyeball comparison at other wavelengths then determines the quality of the overall fit.

Once the best fit has been determined several other interesting quantities can be derived.

(i) $(\alpha+\beta)$, the total extinction at visual wavelengths; $\beta/(\alpha+\beta)$, the relative contribution of "dirty ice" to the total extinction; and A_v/τ_{10}, the ratio of total visual extinction to 10 μm extinction optical depth.

(ii) If d is known we find L from the value of $L/4\pi d^2$. From L and the known value of $\rho_0\delta_g L^{-1/4}$ we determine ρ_0 adopting a suitable value for δ_g (see Section 6). If we assume that the central star has reached the main sequence, the mass/luminosity function gives us M, so that we can determine the mass inflow rate $\dot{M}$, since our basic assumption of free-fall in the dust shell leads to the relation $\dot{M}=4\pi\rho_0(2GM)^{1/2}$.

5. Comparison of Predicted and Observed Spectra for Some Specific Sources

Several infrared point sources of the BN type are presently known. However, only a few of them have been studied in sufficient detail to allow a comparison with the models. We have selected four sources to be fitted with the model spectra of Figure 2: the BN object, OMC 2/IRS 3, RCW 57/IRS 1 and Mon R 2/IRS 2. We did not include the well-known source W 3/IRS 5, because there is recent evidence that this source actually consists of *two* sources, seen along the same line of sight (Neugebauer, private communication).

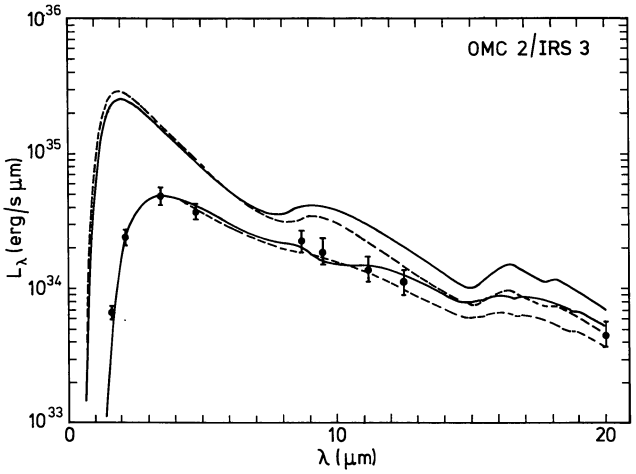

Fig. 5. Theoretical spectra and observations (black dots) for OMC 2/IRS 3. The theoretical fits are based on Spectrum 2 of Figure 2 with $\delta_s/\delta_g=1.5$ (dashed curves) and with $\delta_s/\delta_g=3$ (solid curves). Upper curves are spectra without exterior extinction, lower curves with exterior extinction

i) The BN *Object*

The BN object was discovered in 1967 by Becklin and Neugebauer and studied by means of broad band photometry at 1.65, 2.2, 3.5 and 10 μm. Because their 10 μm band was very broad, the silicate absorption band was not detected at that time. Further broad band photometry was carried out by Low et al. (1970) at 1.65, 2.2, 3.4 and 4.8 μm and by Becklin et al. (1973) at 4.8, 10 and 20 μm. In the latter observations special care was taken to separate the BN object at longer wavelengths (especially at 20 μm) from the nearby confusing Kleinmann-Low nebula. In Figures 3 and 4 the photometric observations of Low et al. and the 20 μm observation of Becklin et al. are shown as open circles. Spectrophotometric data between 2 μm and 2.4 μm were obtained by Penston et al. (1971) (shown in the figures as the dash-dotted curve) and by Gillett and Forrest (1973) between 2.8 μm and 5.6 μm and between 8 μm and 14 μm (shown in the figures as black dots). The latter observations clearly show two absorption features centered at 3.1 μm and 9.8 μm respectively. These absorptions are attributed to spectral features of water ice and silicate. No error bars are shown on the observations. At $\lambda<5$ μm the scatter in the points gives some indication of the observational accuracy; at longer wavelengths the nearby KL nebula could contribute to the flux. The quoted authors estimate that flux values may contain systematic errors of the order of 10% at $\lambda<12$ μm and 20% at about 13 μm in both directions.

We fitted model spectra to the observations using Equation (10) at the reference wavelengths 2.2 μm,

Table 2. Model parameters of accreting young stars

Source	Spectrum no.	$\frac{\delta_s}{\delta_g}$	$L(L_\odot)$	$M(M_\odot)$	A_v	A_v/τ_{10}	$\dot{M}(M_\odot\ yr^{-1})$	$\dot{M}_{cr}(M_\odot\ yr^{-1})$	$\theta_{0.9}$ (arc sec)		
									5 μm	10 μm	20 μm
BN	1*	3	$1.75\ 10^4$	13.5	59	23	$2.3\ 10^{-6}$	$8.2\ 10^{-6}$	$4.2\ 10^{-1}$	1.6	8.8
	2*	3	$1.02\ 10^4$	10.9	49	21	$3.6\ 10^{-6}$	$4.7\ 10^{-6}$	$2.9\ 10^{-1}$	1.0	5.6
	3	3	$5.7\ 10^3$	8.5	35	19.3	$5.5\ 10^{-6}$	$2.5\ 10^{-6}$	$1.8\ 10^{-1}$	$7.2\ 10^{-1}$	3.3
	4	3	$2.9\ 10^3$	6.8	12.3	13.2	$8.3\ 10^{-6}$	$1.22\ 10^{-6}$	$1.2\ 10^{-1}$	$6.0\ 10^{-1}$	2.2
OMC 2/IRS 3	1	3	$4.7\ 10^2$	3.5	38	36	$4.8\ 10^{-7}$	$1.75\ 10^{-7}$	$6.8\ 10^{-2}$	$2.6\ 10^{-1}$	1.4
	2	3	$2.9\ 10^2$	3.0	29	32	$7.8\ 10^{-7}$	$1.04\ 10^{-7}$	$4.9\ 10^{-2}$	$1.7\ 10^{-1}$	$9.4\ 10^{-1}$
	3	3	$1.63\ 10^2$	2.4	15.1	38	$1.21\ 10^{-6}$	$5.6\ 10^{-8}$	$3.0\ 10^{-2}$	$1.2\ 10^{-1}$	$5.7\ 10^{-1}$
RCW 57/IRS 1	1*	3	$5.4\ 10^5$	58	95	20	$1.17\ 10^{-5}$	$2.9\ 10^{-4}$	$3.2\ 10^{-1}$	1.2	6.8
	2*	3	$3.1\ 10^5$	47	85	18.8	$1.76\ 10^{-5}$	$1.60\ 10^{-4}$	$2.2\ 10^{-1}$	$7.7\ 10^{-1}$	4.3
	3*	3	$1.71\ 10^5$	35	72	17.7	$2.6\ 10^{-5}$	$8.8\ 10^{-5}$	$1.3\ 10^{-1}$	$5.5\ 10^{-1}$	2.5
	4*	3	$8.6\ 10^4$	26	49	15.5	$3.8\ 10^{-5}$	$4.3\ 10^{-5}$	$8.9\ 10^{-2}$	$4.5\ 10^{-1}$	1.7
Mon R2/IRS 2	1*	1.5	$1.53\ 10^4$	13.0	74	27	$2.2\ 10^{-6}$	$7.1\ 10^{-6}$	$2.2\ 10^{-1}$	1.0	5.1
	2*	1.5	$9.0\ 10^3$	10.3	65	25	$3.4\ 10^{-6}$	$4.1\ 10^{-6}$	$1.5\ 10^{-1}$	$6.5\ 10^{-1}$	3.2
	3	1.5	$5.1\ 10^3$	8.5	53	23	$5.4\ 10^{-6}$	$2.2\ 10^{-6}$	$9.7\ 10^{-2}$	$4.2\ 10^{-1}$	2.0
	4	1.5	$2.7\ 10^3$	6.7	34	19.5	$8.1\ 10^{-6}$	$1.13\ 10^{-6}$	$6.3\ 10^{-2}$	$2.7\ 10^{-1}$	1.3

*Models are dynamically not allowed.

4.8 μm and 10 μm. In Figure 3 some fits are shown together with the observations. The upper curves are the intrinsic spectra without the exterior extinction; the dashed curve is the normalized Spectrum 1 of Figure 2 with $\delta_s/\delta_g=1.5$, the solid curve is Spectrum 1 of Figure 2 with $\delta_s/\delta_g=3$. The lower curves are the model spectra after correction for exterior extinction. If we adopt a distance $d=500$ pc, parameters resulting from the fit are: $L=1.65\ 10^4 L_\odot$, $A_v=58$ mag and $A_v/\tau_{10}=26$ mag in the case that $\delta_s/\delta_g=1.5$; values of the parameters for the case $\delta_s/\delta_g=3$ are given in Table 2. Good agreement with the observations can be obtained at all wavelengths $\lambda \lesssim 20$ μm. The agreement is better for $\delta_s/\delta_g=3$ than for $\delta_s/\delta_g=1.5$.

The predicted shape of the 10 μm profile of even the best fit in Figure 3 deviates from the observed one; between 8 μm and 9.5 μm the predicted luminosities are about 40% lower than the observed luminosities. The simplest explanation is that our adopted shape of the 10 μm silicate feature is not entirely correct. A similar conclusion was obtained from a comparison of observed and calculated spectra of late-type (super) giants (Bedijn, 1977a, b). There it was suggested that a 10 μm silicate profile steeper between 8 μm and 10 μm and less steep between 10 μm and 13 μm is probably more accurate than the presently used profile due to Gillett et al. (1975b).

The good agreement between predicted and observed spectra for the BN object as shown in Figure 3 unfortunately does not imply that the intrinsic spectrum of the form of Spectrum 1 in Figure 2 is the only one possible. As an illustration we show as the dashed curve in Figure 4 a predicted BN spectrum obtained by applying a somewhat different amount of foreground extinction to an intrinsic spectrum of the form of Spectrum 4 in Figure 2 (with $\delta_s/\delta_g=3$). The parameters resulting from this fit are also listed in Table 2. Compared with the fit in Figure 3 (and again shown in Figure 4 as the solid curve) the luminosities in the wavelength range between 10 μm and 20 μm are about 10–20% higher. An equally good fit could have been obtained for a somewhat smaller value of δ_s/δ_g.

To illustrate the range of possible luminosities and the range of the parameters describing the exterior extinction we summarize their values in Table 2 based on the use of intrinsic model spectra of the form of the spectra in Figure 2, with $\delta_s/\delta_g=3$. Although the spectra 2–4 do not yield such good fits as Spectrum 1 the derived parameters are a fair representation of possible values. Thus the total luminosity remains undetermined up to a factor of 6, while the visual exterior extinction may be as low as 12 mag and as high as 60 mag. In the last three columns of Table 2 we give the predicted angular

sizes, $\theta_{0.9}$, at the wavelengths indicated, for each model fit to the BN object as we also do for the sources discussed hereafter. Finally we notice that our estimate of the stellar mass does allow the BN object to be of type later than B0. In that case the Brackett line seen by Grasdalen (1976) at the position of the BN object may imply a zone of ionized hydrogen immediately surrounding the star, but unable to expand outward to form a compact H II region.

ii) OMC 2/IRS 3

We next consider the source OMC 2/IRS 3 discovered by Gatley et al. (1974). Their observations are shown in Figure 5 as the black dots (we adopted a distance of 500 pc). Also shown in Figure 5 are the results of model fitting, using the normalized intrinsic Spectrum 2 of Figure 2, with $\delta_s/\delta_g=1.5$ (dashed curves) and with $\delta_s/\delta_g=3$ (solid curves). In the fitting procedure we used the wavelengths 2.2 μm, 3.5 μm and 10 μm as reference points. Upper curves are intrinsic spectra without exterior extinction, lower curves those with exterior extinction. Just as in the case of the BN object, $\delta_s/\delta_g=3$ gives a somewhat better fit to the observations, but again the luminosity between 8 μm and 10 μm seems to be somewhat too low. Note that the exterior absorption of the 10 μm silicate feature cannot completely mask the internal emission. It would be very interesting to see whether detailed spectrophotometry around 10 μm would confirm this. We also calculated fits using the other normalized spectra of Figure 2 with $\delta_s/\delta_g=3$. These fits are equally good as the one shown in Figure 5. Derived parameters, such as the luminosity and mass of the central star, the exterior extinction parameters A_v and A_v/τ_{10} and $\dot{M}$ are given in Table 2. (Normalized Spectrum 4 would require a negative exterior extinction and is therefore physically impossible.)

We would like to stress here the point raised for the first time by Aitken and Jones (1973), that for a determination of τ_{10} from observations, it is required that we know the input spectrum before extinction. This may not be trivial. Our model calculations on OMC 2/IRS 3 (Fig. 5) are a case in point: although we predict a value τ_{10} between 0.5 and 1, the observations give no indication of a 10 μm feature because of almost exact cancellation of emission and absorption.

iii) RCW 57/IRS 1

The IR source RCW 57/IRS 1 has been observed by Frogel and Persson (1974). Observations are shown as black dots in Figure 6. The broad band measurement at 10 μm is shown as an open circle. Fits to the observations are obtained using the normalized Spectra 2 of Figure 2 with $\delta_s/\delta_g=1.5$ (dashed curves) and with $\delta_s/\delta_g=3$ (solid curves). Again the spectrum with $\delta_s/\delta_g=3$ gives a somewhat better fit to the observations, although in this case the predicted 12.7 μm luminosity is too small. Various fits using the other normalized spectra of Figure 2 with $\delta_s/\delta_g=3$ are as good as the one shown in Figure 6. The various parameters obtained from the fitting procedure are listed in Table 2 for a distance of 3.6 kpc. Note that the predicted 3.5 μm luminosity is considerably larger than the observed one. This could indicate the presence of a strong 3.1 μm water ice absorption band. It seems worthwhile to confirm this with spectrophotometric observations.

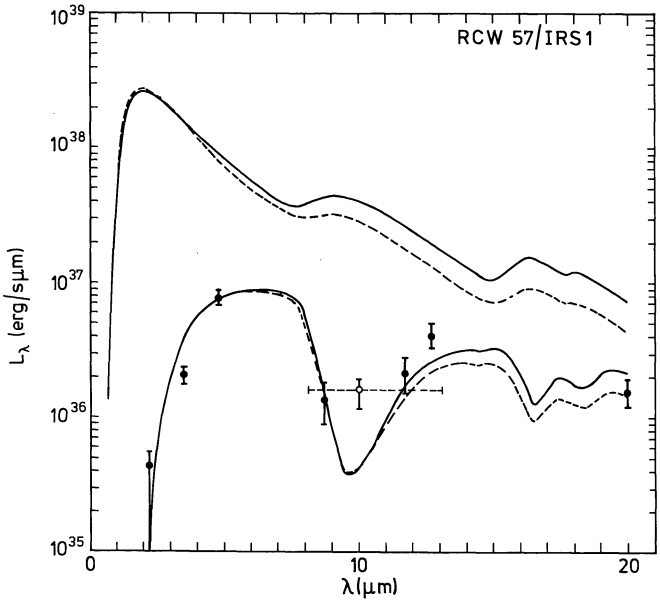

Fig. 6. The same as Figure 5 for RCW 57/IRS 1. The fits are based on Spectrum 2 of Figure 2 with $\delta_s/\delta_g=3$ (solid curves) and with $\delta_s/\delta_g=1.5$ (dashed curves)

iv) Mon R2/IRS 2

Finally we discuss the source Mon R2/IRS 2. The observations (Beckwith et al., 1976) are shown as black dots in Figure 7. Contrary to the previous sources best fits are obtained with normalized spectra with $\delta_s/\delta_g=1.5$. Figure 7 contains a predicted spectrum based on normalized Spectrum 2 and $\delta_s/\delta_g=1.5$. Overall agreement is good, although the observed 10 μm absorption band seems shifted towards longer wavelengths when compared with the predicted one. Probably a better agreement between model and observations could have been obtained if we had used the silicate 10 μm profile as derived by Bedijn (1977a, b). Table 2 lists some derived parameters for fits, obtained with the normalized spectra of Figure 2 with $\delta_s/\delta_g=1.5$ and for a distance of 950 pc.

6. Discussion

Table 2 summarizes the properties and parameters of our best fits to the observed spectra of the BN object, OMC 2/IRS 3, RCW 57/IRS 1 and Mon R2/IRS 2. As

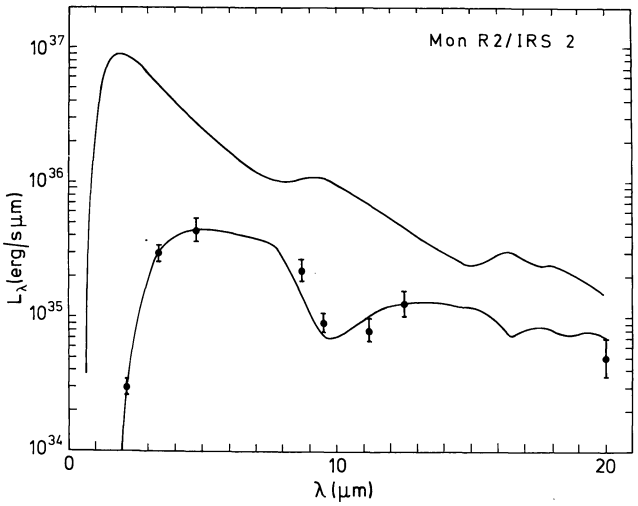

Fig. 7. The same as Figure 5 for Mon R 2/IRS 2. The fit is based on Spectrum 2 of Figure 2 with $\delta_s/\delta_g=1.5$

discussed in the previous section several sets of parameters produce equally good fits. At the moment we cannot use the predicted angular sizes of the sources listed in Table 2 to restrict the range of possible models because i) the resolving power of present day instrumentation is too small at $\lambda \lesssim 10$ μm; ii) strong background radiation is present at $\lambda \gtrsim 10$ μm; iii) the relevant observations have not been made. However, the parameters, A_v/τ_{10} and $\dot{M}$, can possibly be used to restrict the range of models. In Table 2 A_v/τ_{10} varies from 13 to 38. Independent measurements of A_v/τ_{10} exist towards the star VI Cygni 12 where Gillett et al. (1975a) found $A_v/\tau_{10}=14$ and towards several compact H II regions (Gillett et al., 1975b) where it is found that A_v/τ_{10} ranges from 10 to 30. These values are probably typical for the extinction in dark dust clouds. It appears that the values of A_v/τ_{10} that can be derived from our models in Table 2 are consistent with the observations. Although the observed values of A_v/τ_{10} are quite uncertain yet, it appears that the rather safe assumption that $A_v/\tau_{10}>10$ puts a lower limit to the luminosity of allowed models.

We have also investigated whether some of our fits are perhaps dynamically impossible. For this purpose we have calculated the mass inflow rates $\dot{M}$ from the model parameters, as discussed in Section 4. We have adopted a dust-to-gas mass ratio of graphite $\delta_g=2\ 10^{-3}$, derived from a theoretical fit of the general interstellar extinction curve by Tielens and de Jong (1977). An upper limit of $\delta_g=3\ 10^{-3}$ can be derived on the basis of the cosmic abundance of carbon. The mass M of the central star (given in Column 5 of Table 2) that enters into the determination of $\dot{M}$ is found from a mass-luminosity relation constructed from a series of massive main-sequence star models calculated by Papaloizou (1973).

As shown by Kahn (1974) steady inflow around a newly-formed main-sequence star is dynamically possible only if the mass inflow rate $\dot{M}$ exceeds a certain critical value $\dot{M}_{cr}$. Otherwise the flow is reversed by radiation pressure and the accretion is stopped. The dynamics of accreting dust-gas cocoons around massive main-sequence stars has recently been reinvestigated by Bedijn (1977a). He gives a very simple estimate of the critical mass inflow rate that is sufficiently accurate for our purpose. The derivation of this simple expression for $\dot{M}_{cr}$ is given in the Appendix [Eq. (A11)] and values of $\dot{M}_{cr}$ are given in the ninth column of Table 2. If we impose the restriction that $\dot{M}>\dot{M}_{cr}$ a large fraction of the models listed in Table 2 turns out to be dynamically impossible. These models are labelled with an asterisk.

We can therefore exclude models with high luminosities because of the condition $\dot{M}>\dot{M}_{cr}$. Also we can eliminate low luminosity models because of the condition $A_v/\tau_{10}>10$. We thus have bracketed in each case the range of permissible models. If we now consider the mass inflow rates that still are permissible we infer that the typical inflow times $(M/\dot{M})$ of the observed four cases are $\geqq 10^6$ yr. These times are much longer than the Kelvin-Helmholtz timescale and are therefore consistent with the assumption that the stars heating the dust shell have reached the main sequence. However, as we will argue now, this long time scale is at variance with the small number of BN type objects known. If we take for the birth rate of stars with $M>8\ M_\odot$ the value 10^{-11} pc^{-2} yr^{-1} (Ostriker et al., 1974) and if we assume that they remain for 10^6 yr ($\approx M/\dot{M}$) in the accretion phase, then we expect to find $30\ D^2$ of these sources within D kpc from the Sun. At present only some 15 of these sources are known out to a distance of, say, 3 kpc. Even allowing for some incompleteness in the detections the discrepancy seems too large, especially since many known nearby regions of active star formation have been thoroughly studied.

The reason so few BN type sources have been detected is probably that our estimate $(M/\dot{M})$ of the lifetime of the accretion phase is wrong. For it seems quite probable that the accretion rate has been much higher in the past; this would lower $M/\dot{M}$ to our acceptable value. Although our reasoning is based on poor statistics we conclude tentatively that BN type objects are actually early type stars at the very end of their accretion phase. Stars earlier in their accretion phase will have larger mass inflow rates and therefore spectra that peak at much longer wavelengths, hence they have remained undetected so far.

If our interpretation of the BN type objects is correct, they belong in a part of the HR diagram close to the main-sequence location for stars with $M\geqq 8\ M_\odot$. In the illustrative HR diagram in a review paper by Strom (1976, Fig. 3-2) the BN type objects would appear at a similar location as the Herbig emission stars, but they would be more massive and, probably, closer to the main sequence.

Acknowledgements. Bedijn acknowledges partial support by a grant from the Netherlands Organization for the Advancement of Pure Science (Z.W.O.). We thank Dr Friso Olnon for helpful discussions and assistance during the study.

Appendix

Critical Mass Inflow

We consider a spherically symmetric accretion envelope, containing gas and dust, around a central main-sequence star. If we neglect gravitational forces, a dust grain at its melting surface with radius r_m is subject to two competing forces:

(i) the outward-directed radiation pressure force due to the stellar radiation field

$$F_r=\pi a^2 Q_0 L/4\pi c r_m^2 \tag{A1}$$

where a is the dust grain radius and Q_0 is the absorption efficiency of a dust grain for the radiation of the central star of luminosity L, and

(ii) the inward-directed drag force due to gas that is streaming past the dust grain

$$F_d=\pi a^2 \rho_m u_m^2, \tag{A2}$$

where ρ_m is the gas density at r_m and u_m is the relative velocity of gas and dust at r_m (assumed to be much larger than the thermal velocity of the gas atoms/molecules).

We assume that the envelope is in free-fall in a gravitational field dominated by the central star of mass M and that the accretion rate $\dot{M}$ is constant (steady inflow). Then we have

$$v(r)=(2GM/r)^{1/2} \tag{A3}$$

and

$$\dot{M}=4\pi r^2 \rho(r) v(r). \tag{A4}$$

For inflow to continue we require that a dust grain can reach its melting surface, since otherwise dust grains will pile up and a stationary solution is no longer possible. Thus we require

$$F_d \geqq F_r. \tag{A5}$$

Combining Equations (A1)–(A5) and assuming that the dust grain is at rest at its melting surface $[u_m=v(r_m)]$ we can write this condition as

$$\dot{M} \geqq \dot{M}_{cr}=\frac{Q_0 L r_m^{1/2}}{c(2GM)^{1/2}}. \tag{A6}$$

The position of the melting surface of a dust grain can be found from a consideration of its thermal balance at the melting temperature T_m

$$\frac{\pi a^2 L Q_0}{4\pi r_m^2}=4\pi a^2 Q_p(T_m)\sigma T_m^4, \tag{A7}$$

where $Q_p(T_m)$ is the Planck averaged infrared absorption efficiency of the dust grain at T_m and σ is the Stefan-Boltzmann constant. Writing

$$Q_p(T)=qaT^n, \tag{A8}$$

where n and q are parameters characterizing the dust material, we find

$$r_m=\left(\frac{LQ_0}{16\pi\sigma q a T_m^{4+n}}\right)^{1/2}, \tag{A9}$$

and inserting this in Equation (A6) we finally obtain

$$\dot{M}_{cr}=\frac{Q_0^{5/4}}{cT_m}(16\pi\sigma q a T_m^n)^{-1/4} L^{5/4}(2GM)^{-1/2}. \tag{A10}$$

Of the dust grains in the infalling gas-dust mixture, graphite grains have the highest melting temperature. Thus the critical condition is determined by graphite grains at their melting surface. Inserting $q=6.9\ 10^{-2}$ cm $K^{-5/3}$, $n=5/3$ (Kellmann and Gaustad, 1969), $Q_0=1$, $a=2\ 10^{-6}$ cm, and $T_m=2000$ K we obtain

$$\dot{M}_{cr}=1.50\ 10^{-10}(L/L_\odot)^{5/4}(M/M_\odot)^{-1/2}\ M_\odot\ \mathrm{yr}^{-1}. \tag{A11}$$

More sophisticated treatments by Kahn (1974) and by Bedijn (1977a), incorporating the radiation pressure on the grains due to the trapped infrared radiation field in the dust shell yield estimates which are about a factor of 2 larger. Only for $\dot{M}_{cr} \geqq 5\ 10^{-4}\ M_\odot\ \mathrm{yr}^{-1}$ does expression (A11) break down because then the critical condition is completely dominated by the trapped infrared radiation field.

References

Aannestad, P. A., Purcell, E. M.: 1973, *Ann. Rev. Astron. Astrophys.* **11**, 309
Aitken, D. K., Jones, B.: 1973, *Astrophys. J.* **184**, 127
Appenzeller, I., Tscharnuter, W.: 1974, *Astron. Astrophys.* **30**, 423
Becklin, E. E., Neugebauer, G.: 1967, *Astrophys. J.* **147**, 799
Becklin, E. E., Neugebauer, G., Wynn-Williams, C. G.: 1973, *Astrophys. J. Letters* **182**, L7
Beckwith, S., Evans II., N. J., Becklin, E. E., Neugebauer, G.: 1976, *Astrophys. J.* **208**, 390
Bedijn, P. J.: 1977a, Ph. D. Thesis, University of Leiden
Bedijn, P. J.: 1977b, in preparation
Bedijn, P. J., Habing, H. J., de Jong, T.: 1977, paper presented at Symposium on "Recent results in infrared astrophysics", NASA-Ames
Cochran, W. D., Ostriker, J. P.: 1977, *Astrophys. J.* **211**, 392
Davidson, K., Harwit, M.: 1967, *Astrophys. J.* **148**, 443
Finn, G. D., Simon, Th.: 1977, *Astrophys. J.* **212**, 472
Frogel, J. A., Persson, S. E.: 1974, *Astrophys. J.* **192**, 351
Gatley, I., Becklin, E. E., Mathews, K., Neugebauer, G., Penston, M. V., Scoville, N.: 1974, *Astrophys. J. Letters* **191**, L121
Gillett, F. C., Forrest, W. J.: 1973, *Astrophys. J.* **179**, 483
Gillett, F. C., Jones, T. W., Merrill, K. M., Stein, W. A.: 1975a, *Astron. Astrophys.* **45**, 77
Gillett, F. C., Forrest, W. J., Merrill, K. M., Capps, R. W., Soifer, B. T.: 1975b, *Astrophys. J.* **200**, 609
Gilra, D. P.: 1971, *Nature* **220**, 237
Grasdalen, G. L.: 1976, *Astrophys. J. Letters* **205**, L83
Greenberg, J. M., Hong, S. S.: 1974, in IAU Symp. No. 60. F. J. Kerr and S. C. Simonson eds., p. 75

Hong, S. S.: 1975, Ph. D. Thesis, State University of New York at Albany
van de Hulst, H. C.: 1949, *Rech. Astron. Obs. d'Utrecht* **11**, Part 2
van de Hulst, H. C.: 1957, Light scattering by small particles, Wiley, New York
Jones, T. W., Merrill, K. M.: 1976, *Astrophys. J.* **209**, 509
Kahn, F. D.: 1974, *Astron. Astrophys.* **37**, 149
Kellmann, S. A., Gaustad, J. E.: 1969, *Astrophys. J.* **157**, 1465
Larson, R. B.: 1969a, *Monthly Notices Roy. Astron. Soc.* **145**, 271
Larson, R. B.: 1969b, *Monthly Notices Roy. Astron. Soc.* **145**, 297
Larson, R. B.: 1972, *Monthly Notices Roy. Astron. Soc.* **157**, 121
Larson, R. B., Starrfield, S.: 1971, *Astron. Astrophys.* **13**, 190
Low, F. J., Johnson, H. L., Kleinmann, D. E., Latham, A. S., Givel, S. L.: 1970, *Astrophys. J.* **160**, 531
Matthews, H. E., Goss, W. M., Winnberg, A., Habing, H. J.: 1977, *Astron. Astrophys.* (submitted)
Mihalas, D.: 1970, Stellar Atmospheres, W. H. Freeman and Company, San Francisco
Ostriker, J. P., Richstone, O. O., Thuan, T. X.: 1974, *Astrophys. J. Letters* **188**, L8
Papaloizou, J. C. B.: 1973, *Monthly Notices Roy. Astron. Soc.* **162**, 143
Penston, M. V., Allen, D. A., Hyland, A. R.: 1971, *Astrophys. J. Letters* **170**, L33
Pollack, J. B., Toon, O. B., Khare, B. N.: 1973, *Icarus* **19**, 372
Rieke, G. H.: 1974, *Astrophys. J. Letters* **193**, L81
Savage, B. D.: 1976, *Astrophys. J.* **199**, 92
Soifer, B. T., Russell, R. W., Merrill, K. M.: 1976, *Astrophys. J.* **210**, 334
Strom, S. E.: 1976, in *Frontiers of Astrophysics,* E. H. Avrett, ed., Harvard University Press, Cambridge, Mass., p. 95
Taft, E. A., Phillipp, H. R.: 1965, *Phys. Rev.* **138A**, 197
Tielens, A. G. G. M., de Jong, T.: 1977, in preparation
Westbrook, C. K., Tarter, C. B.: 1975, *Astrophys. J.* **200**, 48